 CMES, vol.37, no.2, pp.175-202, 2008

Topological Shape Optimization of Electromagnetic Problems using Level Set Method and Radial Basis Function

Hokyung Shim[1], **Vinh Thuy Tran Ho**[1]
Semyung Wang[1,2] **and Daniel A. Tortorelli**[3]

Abstract: This paper presents a topological shape optimization technique for electromagnetic problems using a level set method and radial basis functions. The proposed technique is a level set (LS) based optimization dealing with geometrical shape derivatives and topological design. The shape derivative is computed by an adjoint variable method to avoid numerous sensitivity evaluations. A level set model embedded into the scalar function of higher dimensions is propagated to represent the design boundary of a domain. The level set function interpolated into a fixed initial domain is evolved by using the Hamilton-Jacobi equation. The moving free boundaries (dynamic interfaces) represented in the level set model determine the optimal shape via the topological changes. In order to improve efficiency of the level set evolution, a radial basis function (RBF) is introduced. The RBF allows the algorithm to create new holes inside the material domain, which lead to an approximately global optimum point. The optimization technique is illustrated using 2D examples captured from 3D level set configuration and the resulting optimum shape is compared with the conventional topology optimization. This work highlights that the derived shape sensitivity is verified using the finite difference method (FDM) through an example, and the level set method is validated as a promising optimization tool in a practical electromagnetic problem. Also, the level set based optimization shows a clear void-solid pattern without gray areas that the topology optimization yields.

Keyword: Shape optimization, level set method, radial basis function, gradient-based optimization, shape derivative.

[1] Dept. of Mechatronics, Gwangju Institute of Science and Technology, Gwangju, 500-712, Korea.
[2] Corresponding author, Email: smwang@gist.ac.kr
[3] Dept. of Mechanical Science and Engineering, University of Illinois at Urbana-Champaingn, Urbana, IL 61801, USA.

1 Introduction

In shape optimization, the design variables directly control the exterior and interior boundary shapes of the structures. Shape optimizations allow more explicit representations of any features that should be incorporated in the design. However, such a boundary representation often has severe limitations: computational cost due to mesh re-generation, tendency of convergence to local minima, and inconvenient compatibility for complex geometrical problems. Furthermore, the shape optimization [Sokolowski and Zolesio (1992)] can not create new holes, which aims at improving the existent designs.

However, topology optimization, which was introduced a few decades ago by Bendsoe and Kikuchi [Bendsoe and Kikuchi (1988)], focuses on obtaining an initial conceptual design. The topology optimization technique [Bendsoe and Sigmund (2003)] can help an engineer who wishes to or needs to design something from inception. It does not require a sophisticated initial design, but rather only requires enough geometric information to define boundary conditions. Seeing the final pattern from the topology optimization, engineers can obtain much information to prepare the design. The topology optimization technique is now sufficiently mature and can be extended to various physical systems [Sigmund (2001); Bendsoe and Sigmund (2003); Yoon and Kim (2005); Cisilino (2006); Zhou and Wang (2006); Shim, Moon, and Wang (2006); Shim, Wang, and Hameyer (2007); Juan, Shuyao, Yuanbo, and Guangyao (2008); Li and Atluri (2008a, 2008b); Shim, Moon, Wang, and Hameyer (2008)]. The topology optimization has typical difficulties, such as gray areas and checkerboard patterns. Optimized topologies with those problems are hard to be manufactured in industry. The checkerboard pattern refers to the formation of regions alternating solid and void elements ordered in a checkerboard-like pattern [Bendsoe (1995); Bendsoe and Sigmund (2003)]. The checkerboards are eliminated if a length scale (by perimeter control or filters) is introduced into the optimization [Sigmund and Petersson (1998); Wang, Lim, Khoo, and Wang (2008)].

In order to overcome the problems that occur in conventional shape and topology optimizations, the level set (LS) based optimization [Sethian and Wiegmann (2000); Wang, Lim, Khoo, and Wang (2007a, 2007b, 2007c); Luo, Wang, Wang, and Wei (2008); Xia and Wang (2008)] has become an attractive tool for optimization techniques in mechanical structure designs. However, it has yet to be introduced in electromagnetic field. The level set method first suggested by Osher and Sethian [Osher and Sethian (1988)] in 1988 has been attractive for computer science. Over the years, the level set method has been effective and successfully applied to structural optimal designs. Sethian et al. [Sethian and Wiegmann (2000)] investigated a new implementation of the level set method for shape optimization.

In their paper, the explicit jump immersed interface method was employed to compute a 2D linear elastostatic equation, and the design model was updated via a material removal-addition scheme without mesh regeneration. This article was the first attempt to apply the level set method of Osher et al. to structural optimization. Allaire et al. [Allaire, Jouve, and Toader (2002); Allaire, Jouve, and Toader (2004)] proposed an implementation of the level set method for structural optimization by employing an adjoint variable method. The shape derivative [Sokolowski and Zolesio (1992)] was used to define the normal velocity (front velocity) of the moving free boundary (dynamic interface). The front propagation was performed by solving the Hamilton-Jacobi equation. The algorithm created no holes inside the domain and converged to a local minimum that depends strongly on the initial estimate [Allaire, Jouve, and Toader (2004); Burger, Hackl and Ring (2004)]. Wang et al. [Wang, Wang, and Guo (2003)] developed a numerical procedure for topology optimization using the level set model by implicitly embedding the structural boundary into a higher order (one dimension higher) scalar function. Xia et al. [Xia and Wang (2008)] extended this method to thermoelastic structural problem. Wang et al. [Wang and Wang (2006a); Wang, Lim, Khoo, and Wang (2007c, 2007d)] applied radial basis functions to the level set based structural topology optimization. The unconstrained optimization problem using a presumed Lagrange multiplier was performed to show possibility. Furthermore, the radial basis functions were applied to geometry projection method [Norato, Haber, Tortorelli, and Bendsoe (2004)] for optimizing photonic nanostructures [Frei, Tortorelli, and Johnson (2007)]. However, most researches have not shown sensitivity validation, even in simple examples.

In this paper, a level set (LS) based optimization is presented for electromagnetic problems and compared with the conventional topology optimization based on the solid isotropic microstructure with penalization (SIMP). A mathematical model for electromagnetic system is formulated for a general optimization problem with one objective function subject to specified constraint (volume fraction). In order to calculate the normal velocity, the shape sensitivity is derived by employing the adjoint variable method, which reduces numerous sensitivity evaluations regardless of the number of design variables. The derived sensitivity formula is validated using the finite difference method. Two examples are investigated to demonstrate the strength of the topological shape optimization.

2 Introduction of Electromagnetic Field

When the displacement currents are neglected, electromagnetic fields can be described using the set of Maxwell's equations:

$$\nabla \times H_{mag} = J_T \tag{1}$$

$$B_{mag} = \mu H_{mag}, \quad (\mu = \mu_r \mu_0) \tag{2}$$

$$\nabla \cdot B_{mag} = 0 \tag{3}$$

where H_{mag}, J_T, B_{mag}, μ, μ_r, and μ_0 are the magnetic field intensity, total current density, magnetic flux density, permeability of the material, relative permeability of the material, and permeability of the air $[4\pi \times 10^{-7}]$, respectively.

In the electromagnetic field, all parts of the total current density vector J_T, are considered as:

$$J_T = J_s + \sigma v \times B_{mag} \tag{4}$$

where J_s, σ and v are the applied source current density vector, electric conductivity, and velocity of the conductor with respect to the magnetic flux density, respectively.

In this paper, it is assumed that there is no conductor motion. By introducing a vector potential, A, B_{mag} is defined as:

$$\nabla \times A = B_{mag} \tag{5}$$

and identically satisfies (3). Through eliminating H_{mag} in (1) and (2) and substituting (5), a single equation for the electromagnetic field is consequently simplified to:

$$\nabla \times (\frac{1}{\mu} \nabla \times A) = J_s \tag{6}$$

In order to obtain a unique solution to an electromagnetic problem, either a known value of A or its normal derivative must be specified at each point on the boundary. If the potential is specified as constant along the boundary, it becomes an equipotential. Furthermore, the normal derivative of the potential is specified by default as a result of discarding the surface integral on the boundary [Salon (1998)].

Consider an electromagnetic body occupying an open domain, Ω, bounded by a closed surface, Γ, as shown in Fig. 1. All material properties are assumed isotropic in the domain. The boundary conditions are composed of a zero magnetic vector potential boundary, Γ_0, and a magnetic flux boundary, Γ_1, as follows:

$$\Gamma_0 \cup \Gamma_1 = \Gamma \tag{7}$$

The boundary conditions of the magnetic field are imposed on the surface:

$$A = 0 \text{ on } \Gamma_0 \text{ (Homogeneous Dirichlet condition)} \tag{8}$$

$$\frac{\partial A}{\partial n} = 0 \text{ on } \Gamma_1 \text{ (Natural boundary condition or Neumann condition)} \tag{9}$$

Here, n is an outward unit vector normal to the boundary.

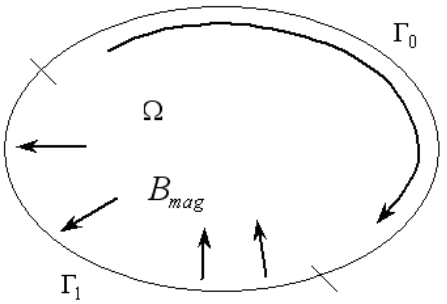

Figure 1: Magnetic field in space

To obtain the variational equation for the magnetic field, multiplying both sides of (6) with the virtual vector potential, $\bar{A}$, and integrating it over the domain yields:

$$\int_\Omega \left[\nabla \times \left(\frac{1}{\mu}\nabla \times A\right)\right] \cdot \bar{A} d\Omega = \int_\Omega [J_s] \cdot \bar{A} d\Omega \text{ for all } \bar{A} \in \tilde{A} \tag{10}$$

where $\tilde{A}$ is the space of the admissible vector potential.

The integrand of the left side of (10) can be expressed as a summation of the domain integral and boundary integral:

$$\begin{aligned}\int_\Omega \left[\nabla \times \left(\frac{1}{\mu}\nabla \times A\right)\right] \cdot \bar{A} d\Omega \\ = \int_\Omega \left[(\nabla \times A) \times \left(\frac{1}{\mu}\nabla \times \bar{A}\right)\right] d\Omega - \int_\Gamma \left[\left(\frac{1}{\mu}\nabla \times A\right) \times n\right] \cdot \bar{A} d\Gamma\end{aligned} \tag{11}$$

The boundary integral of (11) becomes zero by imposing the natural boundary condition on Γ_1 and the kinematically admissible $\bar{A}$ on Γ_0. Then, the final form of the variational equation is:

$$\int_\Omega \left[(\nabla \times A) \cdot \left(\frac{1}{\mu}\nabla \times \bar{A}\right)\right] d\Omega = \int_\Omega \left[J_s \cdot \bar{A}\right] d\Omega \text{ for all } \bar{A} \in \tilde{A} \tag{12}$$

Therefore, in the electromagnetic field, the energy bilinear form $a(\bullet,\bullet)$ and the load linear form $l(\bullet)$ can be used to express (12):

$$a(A,\bar{A}) = \ell(\bar{A}), \quad A|_{\Gamma_0} = 0 \text{ for all } \bar{A} \in \tilde{A} \tag{13}$$

where

$$a(A,\bar{A}) = \int_{\Omega} \left[(\nabla \times A) \cdot (\frac{1}{\mu} \nabla \times \bar{A}) \right] d\Omega \tag{14}$$

$$l(\bar{A}) = \int_{\Omega} \left[J_s \cdot \bar{A} \right] d\Omega \tag{15}$$

3 Conventional Level Set Method of Implicitly Moving Free Boundaries

3.1 Conventional level set method

The boundaries of n-dimensional structure can be implicitly represented by the level set of a scalar valued field. Let Γ^{ω}, shown in Fig. 2, denotes an isosurface of a level set function, Φ. The structural domain ω is interior to Γ^{ω}, i.e.

$$\omega = \{\mathbf{x} : \Phi(\mathbf{x}) > k\} \tag{16}$$

where k is an arbitrary single value (k becomes zero in the zero level set), and $\mathbf{x}$ is a point in an n-dimensional real space, R^n.

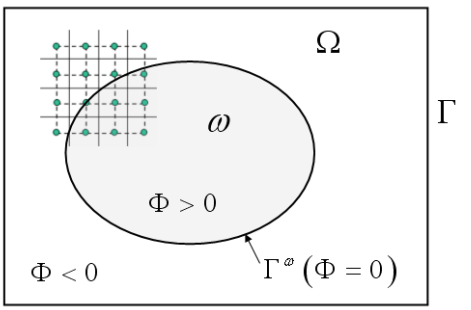

Figure 2: Level set function and variable domain ω embedded in the fixed domain Ω (dashed lines show level set grid and thin solid lines represent fixed finite element grid).

For our purpose, the variable design region ω is embedded in a fixed finite element domain Ω, as shown in Fig. 2 and the level set function Φ is discretized by a rectilinear grid whose the nodes are centered in the fixed finite elements.

A process of topological shape optimization is described by letting the level set function dynamically change in time, so that the variable domain at an arbitrary time, τ, is expressed as:

$$\omega_\tau = \{\mathbf{x}_\tau : \ \Phi(\mathbf{x}_\tau, \tau) > k\} \tag{17}$$

By differentiating both sides of the level set equality $\Phi(\mathbf{x}_\tau, \tau) = k$ with respect to the parameter τ and applying the chain rule, the Hamilton-Jacobi equation is obtained:

$$\left.\frac{\partial \Phi(\mathbf{x}_\tau, \tau)}{\partial \tau}\right|_{\tau=0} + \nabla\Phi(\mathbf{x}_\tau, \tau)|_{\tau=0} \cdot \left.\frac{d\mathbf{x}_\tau}{d\tau}\right|_{\tau=0} = 0 \tag{18}$$

This equation governs the motion of the boundary parts on Γ^{ω_τ}. The explicit shape evolves according to a fictitious time that corresponds to a descent stepping. For traditional reasons, we define the valued boundary velocity $\mathbf{V}$ as:

$$\frac{d\mathbf{x}_\tau}{d\tau} = \lim_{\tau \to 0} \frac{\mathbf{x}_\tau - \mathbf{x}}{\tau} = \mathbf{V}(\mathbf{x}, 0) = \mathbf{V}(\mathbf{x}) \tag{19}$$

Substituting (19) into (18) at a fictitious time results in:

$$\frac{\partial \Phi(\mathbf{x})}{\partial \tau} + \nabla\Phi(\mathbf{x}) \cdot V(\mathbf{x}) = 0 \tag{20}$$

By introducing a normal velocity, V_n, perpendicular to the boundary, Γ^ω, (20) becomes:

$$\frac{\partial \Phi}{\partial \tau} = V_n |\nabla\Phi| \tag{21}$$

where

$$V_n = \mathbf{V} \cdot \mathbf{n} = -\mathbf{V}(x) \cdot \frac{\nabla\Phi}{|\nabla\Phi|}, \text{ and } V_t = 0 \tag{22}$$

We do not consider the tangential velocity, V_t, since it does not move the boundary. In the conventional level set method [Wang, Wang, and Guo (2003)], the level set function, Φ, evolves at each time step with a normal velocity field $V_n(x)$ by solving the first-order partial differential equation (PDE) of (21). In our level set application, the velocity field is used to transform ω into the optimal design ω^*. A highly robust and accurate computational method developed by Osher and Sethian [Osher and Sethian (1988)], called the "upwind scheme", is employed for a discrete

solution of (21) to manage overshooting problem. It is based on the finite difference approach [Jiang and Peng (2000)].

$$\Phi_{ij}^{n+1} = \Phi_{ij}^{n} - \Delta t[\max(V_{n_{ij}},0)\nabla^{+} + \min(V_{n_{ij}},0)\nabla^{-}] \tag{23}$$

where

$$\nabla^{+} = [\max(D_{ij}^{-x},0)^2 + \min(D_{ij}^{+x},0)^2 + \max(D_{ij}^{-y},0)^2 + \min(D_{ij}^{+y},0)^2]^{1/2} \tag{24}$$

$$\nabla^{-} = [\max(D_{ij}^{+x},0)^2 + \min(D_{ij}^{-x},0)^2 + \max(D_{ij}^{+y},0)^2 + \min(D_{ij}^{-y},0)^2]^{1/2} \tag{25}$$

Here, Δt is a time step, and $D_{ij}^{\pm x}$ and $D_{ij}^{\pm y}$ are the forward and backward difference operators in the dimensions of $x \in R^2$, respectively. In addition, the time steps, Δt must be limited to ensure the stability of the upwind scheme.

3.2 Formulation of topological shape optimization by the conventional level set method

The objective of a topological shape optimization is to find an optimal layout (region) to maximize the magnetic energy stored in the system (especially in the air-gap region of magnetic actuators) under the prescribed electromagnetic loadings. The magnetic energy density is defined as follows:

$$\prod(A) = \frac{1}{2} B_{mag} H_{mag} \tag{26}$$

As such, the design optimization problem takes the form:

Minimize an objective function J:

$$J(A;\Phi) = \int_{\Omega} \xi(A;\Phi) d\Omega = -\int_{\Omega} \prod(A) H(\Phi) d\Omega \tag{27}$$

Subject to:

$$a(A,\bar{A};\Phi) = l(\bar{A};\Phi), \quad A|_{\Gamma_0} = 0, \text{ for all } \bar{A} \in \tilde{A} \tag{28}$$

in which

$$a(A,\bar{A};\Phi) = \int_{\Omega} \left[(\nabla \times A) \cdot (\frac{1}{\mu} \nabla \times \bar{A}) H(\Phi) \right] d\Omega \tag{29}$$

$$l(\bar{A};\Phi) = \int_{\Omega} \left[J_s \cdot \bar{A} \cdot H(\Phi) \right] d\Omega \tag{30}$$

$$g(\Phi) = V(\Phi) - V_{\max} \le 0, \quad V(\Phi) = \int_{\Omega} H(\Phi) d\Omega \tag{31}$$

where H is the approximate Heaviside step function (see equation (79)), g is a constraint function, V is the volume, $V_{\max}$ is the allowable volume, and Φ is the level set function (see numerical implementation (78)).

3.3 Adjoint design sensitivity analysis

The aim of this section is to develop the shape derivative of $J(A;\Phi)$ in (27). Since the complex variable geometry, ω is embedded in the fixed domain, Ω, a proxy analysis problem is formulated on Ω. First of all, taking the Fréchet derivative of $a(A,\bar{A};\Phi)$ with respect to τ in the direction of the normal velocity yields [Sokolowski and Zolesio (1992); Haug, Choi, and Komkov (1986)]:

$$\begin{aligned} a' &= \frac{d}{d\tau} a_{\Phi+\tau\delta\Phi}(A(x;\Phi+\tau\delta\Phi),\bar{A})\Big|_{\tau=0} \\ &= a'_{\delta\Phi}(A,\bar{A};\Phi) + a_{\Phi}(A',\bar{A};\Phi) \end{aligned} \tag{32}$$

where

$$a'_{\delta\Phi}(A,\bar{A};\Phi) = \int_{\Omega} (\nabla\times A)\cdot(\frac{1}{\mu}\nabla\times\bar{A})\delta(\Phi)\,d\Omega \tag{33}$$

$$a_{\Phi}(A',\bar{A};\Phi) = l'_{\delta\Phi}(\bar{A};\Phi) - a'_{\delta\Phi}(A,\bar{A};\Phi) \tag{34}$$

where $\delta(\Phi)$ is the Dirac delta function (see equation (80)) with respect to the Φ, which is obtained by the derivative of $H(\Phi)$.

The Fréchet derivative of $l(\bar{A};\Phi)$ with respect to τ in the direction is expressed as:

$$l' = \frac{d}{d\tau} l_{\Phi+\tau\delta\Phi}(\bar{A})\Big|_{\tau=0} = l'_{\delta\Phi}(\bar{A};\Phi) = \int_{\Omega} J_s\bar{A}\delta(\Phi)d\Omega \tag{35}$$

The Fréchet derivative of $J(A;\Phi)$ is written as:

$$\begin{aligned} J' &= \frac{d}{d\tau} J_{\Phi}(A(x;\Phi+\tau\delta\Phi))\Big|_{\tau=0} \\ &= \int_{\Omega} \left[\xi'_{\delta\Phi}(A;\Phi) + \xi_{\Phi}(A';\Phi)\right] d\Omega + \int_{\Gamma} \xi(A;\Phi)V_n d\Gamma \end{aligned} \tag{36}$$

where the first two terms of the right side of (36) are given as:

$$\int_{\Omega} \xi'_{\delta\Phi}(A;\Phi)d\Omega = -\int_{\Omega} \Pi(A)\delta(\Phi)\,d\Omega \tag{37}$$

$$\begin{aligned} \int_{\Omega} \xi_{\Phi}(A';\Phi)d\Omega &= -\int_{\Omega} \Pi(A')H(\Phi)\,d\Omega \\ &= -a_{\Phi}(A',\lambda;\Phi) \end{aligned} \tag{38}$$

Since there is an implicit dependence term in the design variable, an adjoint magnetic response λ is introduced to simplify the derivative of $J(A;\Phi)$ [Haug, Choi,

and Komkov (1986); Shim, Moon, and Wang (2006)]. The adjoint magnetic system is formulated as:

$$a(\lambda,\bar{\lambda};\Phi)=\int_{\Omega}H(\Phi)J_s\bar{\lambda}\,d\Omega \text{ for all } \bar{\lambda}\in\tilde{A} \tag{39}$$

Since $A'\in\tilde{A}$, (39) can be rewritten as:

$$a(\lambda,A';\Phi)=\int_{\Omega}H(\Phi)J_s\delta A\,d\Omega \text{ for all } A\in\tilde{A} \tag{40}$$

Then, using the adjoint response, (34) can be expressed as:

$$a(A',\lambda;\Phi)=l'_{\delta\Phi}(\lambda;\Phi)-a'_{\delta\Phi}(A,\lambda;\Phi) \tag{41}$$

Since $a(\bullet,\bullet)$ is a symmetric operator, (40) and (41) are equal. By substituting (41) into (38), (36) becomes:

$$\begin{aligned}\frac{dJ}{d\tau}&=\int_{\Omega}\left[-\Pi(A)\delta(\Phi)\right]d\Omega-l'_{\delta\Phi}(\lambda;\Phi)+a'_{\delta\Phi}(A,\lambda;\Phi)+\int_{\Gamma}\xi(A;\Phi)V_n d\Gamma\\&=\int_{\Omega}\left[-\Pi(A)-J_s\lambda+(\nabla\times A)\left(\frac{1}{\mu}\nabla\times\lambda\right)\right]\delta(\Phi)d\Omega+\int_{\Gamma}\xi(A;\Phi)V_n d\Gamma\\&=\int_{\Omega}\Theta(A,\lambda)\delta(\Phi)d\Omega-\int_{\Gamma}\Pi(A)H(\Phi)V_n d\Gamma\end{aligned} \tag{42}$$

Since the geometry in the fixed domain has no movement, the normal velocity on the boundary, Γ, becomes zero. Then (42) is rewritten as:

$$\frac{dJ}{d\tau}=\int_{\Omega}\Theta(A;\lambda)\delta(\Phi)d\Omega \tag{43}$$

3.4 Formula of optimization problem

The Lagrange multiplier method can be applied to solve constrained problems [Arora (1989)]. To transform a constrained problem into an unconstrained optimization formula, a Lagrangian function, Λ, with a positive Lagrange multiplier, l_v, can be given by:

$$\begin{aligned}\Lambda(\Phi,l_v,s)&=J(A;\Phi)+l_v\left(g(\Phi)+s^2\right)\\&=-\int_{\Omega}\prod(A)H(\Phi)d\Omega+l_v\left(\int_{\Omega}H(\Phi)d\Omega-V_{\max}+s^2\right)\end{aligned} \tag{44}$$

where s is a slack variable which is introduced to convert an inequality constraint to an equality constraint.

According to the Kuhn-Tucker condition of the Lagrange theorem, the necessary condition for a minimizer gives:

$$\begin{aligned}\frac{d\Lambda}{d\tau} &= \frac{dJ(A;\Phi)}{d\tau} + l_v \frac{dg(\Phi)}{d\tau} \\ &= \int_\Omega \delta(\Phi)\Theta(A,\lambda)d\Omega + \int_\Omega l_v \delta(\Phi)d\Omega = 0\end{aligned} \tag{45}$$

$$\frac{d\Lambda}{dl_v} = \int_\Omega H(\Phi)d\Omega - V_{\max} + s^2 = 0 \tag{46}$$

$$\frac{d\Lambda}{ds} = 2l_v \cdot s = 0 \tag{47}$$

All derivatives are evaluated at each level set grid. The gradient of the Lagrangian function with respect to τ is the most important term that yields propagation information for the optimization problem. The first term of the right side in (45) is a shape derivative obtained from the adjoint variable method explained in the previous section. The resulting equation of (45) is rewritten as:

$$\int_\Omega \delta(\Phi)\cdot(\Theta(A,\lambda)+l_v)d\Omega = 0 \tag{48}$$

Accordingly, the optimal necessary conditions are summarized and the velocity field is obtained for the boundary variation in the descent direction of the sensitivity as:

$$V_n(x) = -\{\Theta(A,\lambda)+l_v\} \tag{49}$$

The Lagrange multiplier, l_v becomes zero if either the used volume is less than the allowable volume (called an inactive state of optimization), or is equal to the allowable volume, i.e. an active constraint. The evaluation of s allows the optimizer to check the feasibility of the candidate points with respect to the volume constraint. In order to determine the non-zero positive Lagrange multiplier, i.e. the violated volume constraint, it is assumed that the used volume is identical to the allowable volume. With (21) and (22), it leads to:

$$\int_\Omega \delta(\Phi)\,|\nabla\Phi|\,V_n(x)d\Omega = -\int_\Omega \delta(\Phi)\,|\nabla\Phi|\,(\Theta(A,\lambda)+l_v)\,d\Omega = 0 \tag{50}$$

Thus, the Lagrange multiplier is calculated by:

$$l_v = -\frac{\int_\Omega \delta(\Phi)\,|\nabla\Phi|\,\Theta(A,\lambda)d\Omega}{\int_\Omega \delta(\Phi)\,|\nabla\Phi|\,d\Omega} \tag{51}$$

Equation (51) implies that the Lagrange multiplier is the average of the sensitivity along the entire design boundary.

4 Advanced Level Set Method using Radial Basis Function

4.1 Radial basis function applied in the level set method

The level set function $\Phi(\mathbf{x})$ was parameterized using a number of radial basis functions (RBFs). Each RBF, φ_i, is a radially symmetric function centered at a knot identified by its position vector $\mathbf{x}_i$. A single function φ is used to form a family of RBFs. The multiquadric spline, found to be one of the best splines for RBF interpolations [Franke (1982)], is used here with the RBFs. It is written as:

$$\varphi_i(\mathbf{x}) = \varphi(\|\mathbf{x}-\mathbf{x}_i\|) = \sqrt{(\mathbf{x}-\mathbf{x}_i)^2 + c_i^2} \tag{52}$$

where $||.||$ denotes the Euclidean norm [Cheng, Golberg, Kansa and Zammito (2003)], and c_i is the free shape parameter that is commonly assumed to be a constant for all knots i.

Using the RBF parameterization, the level set function is expressed as:

$$\Phi(\mathbf{x}) = \sum_{i=1}^{N} C_i^{\alpha} \varphi_i(\mathbf{x}) + p(\mathbf{x}) \tag{53}$$

where C_i^{α} is the expansion coefficient of the corresponding RBF at the i^{th} knot. $p(\mathbf{x})$ is a first-degree polynomial which, in the 2D problem, can be written as $p(\mathbf{x}) = p_0 + p_1 x + p_2 y$. To ensure a unique parameterization to the RBF interpolation, the expansion coefficients are subject to the constraint:

$$\sum_{i=1}^{N} C_i^{\alpha} = \sum_{i=1}^{N} C_i^{\alpha} x_i = \sum_{i=1}^{N} C_i^{\alpha} y_i = 0 \tag{54}$$

The total linear matrix system is summarized as:

$$\mathbf{U}\boldsymbol{\alpha} = \mathbf{f}, \quad \text{where } \mathbf{U} = \begin{bmatrix} \mathrm{Z} & \boldsymbol{\rho} \\ \boldsymbol{\rho}^T & 0 \end{bmatrix} \tag{55}$$

$$\boldsymbol{\alpha} = [\mathbf{C}^{\alpha}\ \mathbf{p}_j] = \begin{bmatrix} C_1^{\alpha} & \cdots & C_N^{\alpha} & p_0 & p_1 & p_2 \end{bmatrix}^T \tag{56}$$

$$\boldsymbol{f} = \begin{bmatrix} \Phi(\mathbf{x}) & 0 \end{bmatrix} = \begin{bmatrix} \Phi(x_1) & \cdots & \Phi(x_N) & 0 & 0 & 0 \end{bmatrix} \tag{57}$$

and $\mathbf{Z}_{ij} = \varphi_j(\mathbf{x}_i)$ for $(i, j = 1, \cdots, N)$, $\boldsymbol{\rho} = [\boldsymbol{\rho}_1\ \boldsymbol{\rho}_2\ \boldsymbol{\rho}_3] \in R^{N\times 3}$, where $\boldsymbol{\rho}_1 = [1\ \cdots\ 1]^T$, $\boldsymbol{\rho}_2 = [x_1\ \cdots\ x_N]^T$, and $\boldsymbol{\rho}_3 = [y_1\ \cdots\ y_N]^T$. $\mathbf{p}_j$ is the basis for the polynomial.

After calculating the generalized expansion coefficient $\boldsymbol{\alpha}$ in (55), the level set function with the RBF, i.e. (53), is rewritten as:

$$\Phi(\mathbf{x}) = \boldsymbol{\Psi}(\mathbf{x})^T \boldsymbol{\alpha}, \tag{58}$$

where $\mathbf{\Psi}(\mathbf{x}) = [\varphi_1(\mathbf{x}) \ \cdots \ \varphi_N(\mathbf{x}) \ 1 \ x \ y]^T$.

The explicit boundary Γ^{ω} is achieved by propagating the level set, $\Phi(\mathbf{x}) > k$ along its normal directions at each time step.

Unlike the conventional level set method, the space and time in the original Hamilton-Jacobi PDE are completely separable in an advanced level set method.

$$\Phi = \Phi(\mathbf{x}, \tau) = \mathbf{\Psi}(\mathbf{x})^T \boldsymbol{\alpha}(\tau) \tag{59}$$

Substituting (59) into the Hamilton-Jacobi equation (20) yields a dynamic level set model:

$$\mathbf{\Psi}(\mathbf{x})^T \frac{d\boldsymbol{\alpha}(\tau)}{d\tau} + V_n \left| \left(\nabla \mathbf{\Psi}(\mathbf{x})^T \boldsymbol{\alpha} \right) \right| = 0 \tag{60}$$

in which the normal velocity field is given as:

$$V_n = -\frac{\mathbf{\Psi}(\mathbf{x})^T}{|(\nabla \mathbf{\Psi})^T \boldsymbol{\alpha}(\tau)|} \cdot \frac{d\boldsymbol{\alpha}(\tau)}{d\tau} \tag{61}$$

The original time dependent problem is now discretized by the generalized expansion coefficients.

Substituting (55) into (60) yields:

$$\mathbf{U} \frac{d\boldsymbol{\alpha}}{d\tau} + \mathbf{B}(\boldsymbol{\alpha}) = 0 \tag{62}$$

where

$$\mathbf{B}(\boldsymbol{\alpha}) = \left[V_n(x_1) \cdot \left| (\nabla \mathbf{\Psi}^T(x_1)) \boldsymbol{\alpha} \right| \ \ldots \ V_n(x_N) \cdot \left| (\nabla \mathbf{\Psi}^T(x_N)) \boldsymbol{\alpha} \right| \ 0 \ 0 \ 0 \right]^T \tag{63}$$

The solution is obtained by updating the following equation with the time step Δt:

$$\boldsymbol{\alpha}(\tau^{n+1}) = \boldsymbol{\alpha}(\tau^n) - \Delta t \cdot \mathbf{U}^{-1} \mathbf{B}(\boldsymbol{\alpha}(\tau^n)) \tag{64}$$

This equation follows from the first order forward Euler's method, which is the simplest solution algorithm with good accuracy for ordinary differential equations [Wang and Wang (2006a); Wang, Lim, Khoo, and Wang (2007c)].

It is noted that the time step size should be small enough to achieve numerical stability due to the Courant-Friedrichs-Lewy (CFL) condition [Allaire, Jouve, and Toader (2004)].

4.2 Formula of topological shape optimization using adjoint design sensitivity in the advanced level set method

In advanced level set method, the fundamental basis is to parameterize the level set function Φ using the radial basis function φ. For the purpose of the topological shape optimization, we define the objective function J^{rbf} using (59) as:

$$J^{rbf}(A;\Psi^T\alpha) = -\int_\Omega \prod(A)H(\Psi^T\alpha)d\Omega \tag{65}$$

An optimization problem is to maximize the magnetic energy, i.e. (26) generated in the air-gap region as described in section 3.2.

Equation (65) is subject to:

$$a(A,\bar{A};\Psi^T\alpha) = l(\bar{A};\Psi^T\alpha),\ A|_{\Gamma_0} = 0,\ \text{for all}\ \bar{A}\in\tilde{A} \tag{66}$$

in which

$$a(A,\bar{A};\Psi^T\alpha) = \int_\Omega \left[(\nabla\times A)\cdot(\frac{1}{\mu}\nabla\times\bar{A})H(\Psi^T\alpha)\right]d\Omega \tag{67}$$

$$l(\bar{A};\Psi^T\alpha) = \int_\Omega \left[J_s\cdot\bar{A}\cdot H(\Psi^T\alpha)\right]d\Omega \tag{68}$$

$$g^{rbf}(\Psi^T\alpha) = V(\Psi^T\alpha) - V_{\max} \le 0, \quad V(\Psi^T\alpha) = \int_\Omega H(\Psi^T\alpha)d\Omega \tag{69}$$

Here, it is noted that the level set function Φ is replaced by $\Psi^T\alpha$. The derivation procedure for the adjoint design sensitivity analysis in the advanced level set method is same to that of the conventional level set method. The differential term with respect to time is the generalized expansion coefficients. In this way, the space dependence exists in the RBF and the temporal term evolves in the expansion coefficients, since all knots are fixed in the space of the design domain.

In the advance level set method, (58) leads (43) to:

$$\frac{dJ^{rbf}}{d\tau} = \int_\Omega \Theta(A;\lambda)\delta(\Psi^T\alpha)\Psi^T\mathbf{I}_\alpha d\Omega \tag{70}$$

in which

$$\delta(\Psi^T\alpha)\Psi^T\mathbf{I}_\alpha = H'(\Psi^T\alpha) \tag{71}$$

Here, $\mathbf{I}_\alpha$ is the unit vector.

For formula of the optimization problem using the positive Lagrange multiplier, l_v^{rbf}, a Lagrangian function Λ^{rbf}

based on the RBF is defined as:

$$\Lambda^{rbf}(\Psi,\alpha,l_v^{rbf},s) = J^{rbf}(A;\Psi^T\alpha) + l_v^{rbf}(g^{rbf}(\Psi^T\alpha)+s^2) \tag{72}$$

The Kuhn-Tucker condition yields the necessary condition for (72) whose derivative with respect to τ is:

$$\begin{aligned}\frac{d\Lambda^{rbf}}{d\tau} &= \frac{dJ^{rbf}}{d\tau} + l_v^{rbf}\frac{dg^{rbf}}{d\tau} \\ &= \int_\Omega \delta(\Psi^T\alpha)\left[\Theta(A,\lambda)+l_v^{rbf}\right]\Psi^T\mathbf{I}_\alpha d\Omega = 0\end{aligned} \tag{73}$$

In the advanced level set method, the velocity field is calculated via the same procedure to deriving (49). The velocity field is obtained by:

$$V_n^{rbf}(x) = -\{\Theta(A,\lambda)+l_v^{rbf}\} \tag{74}$$

The prescribed assumption that the used volume is identical to the allowable volume is held for the advanced level set method. Using (74), this yields:

$$\int_\Omega \delta(\Psi^T\alpha)\left|\nabla\Psi^T\alpha\right| V_n^{rbf}(x)d\Omega = -\int_\Omega \delta(\Psi^T\alpha)\left|\nabla\Psi^T\alpha\right|\left(\Theta(A,\lambda)+l_v^{rbf}\right)d\Omega = 0 \tag{75}$$

Consequently, the Lagrange multiplier for the advanced level set method is obtained by:

$$l_v^{rbf} = -\frac{\int_\Omega \delta(\Psi^T\alpha)\left|\nabla\Psi^T\alpha\right|\Theta(A,\lambda)d\Omega}{\int_\Omega \delta(\Psi^T\alpha)\left|\nabla\Psi^T\alpha\right|d\Omega} \tag{76}$$

In general, the velocity is obtained from the sensitivity analysis of the prescribed objective function, and the descent direction of the objective is determined by the steepest descent method.

5 Numerical Implementation

The optimization principle is to move the free boundaries represented in a three-dimensional level set configuration according to their sensitivities with respect to an objective function. The moving free boundaries are moved, merged or eliminated in the level set method where the velocity function is derived from a shape sensitivity analysis. By introducing an RBF, the nucleation of new holes for the moving free boundaries is allowed in the given material domain [Wang, Lim, Khoo, and Wang (2007d)]. A scalar level set function, Φ, which is defined over the design domain Ω, represents the dynamic interfaces for the set where $\Phi(X,\tau)=0$. Here, the level set method is described in six steps:

Step 1: Select the design domain, Ω, and initial shapes, ω on the domain.

Step 2: Initialize the scalar level set function, $\Phi(X,0)$, at $\tau = 0$ corresponding to an initial estimate, ω_0.

Step 3: Solve the equilibrium equation (13) to obtain the magnetic vector potential A.

Step 4: Find the adjoint response, λ, of the corresponding adjoint equation (39) and calculate the normal velocity, V_n, at each position $\mathbf{x}$ to propagate of all level sets embedded in the function, $\Phi(X,\tau)$.

Step 5: Compute the velocity (49) and solve the evolving equation (21) (Hamilton-Jacobi equation [Osher and Sethian (1988)]) to update the scalar level set function in the conventional level set method. In order to allow new hole generation in the design domain during the optimization, an interpolation equation of the radial basis function is applied in the advanced level set method, as explained in Section 4. Solution of (64) on the velocity of (74) updates the advanced level set function.

Step 6: Check the convergence using the criteria:

$$J_{\tau+\Delta t} - J_\tau \leq \varepsilon \tag{77}$$

where ε is a small positive value for convergence.

Equation (13) is solved based on a finite element method. Here, the level set function Φ is designed as:

$$\Phi(\mathrm{X}_\tau,\tau) = \begin{cases} +d(\mathrm{X}_\tau,\Gamma_\tau^\omega) & \mathrm{X}_\tau \in \omega_\tau \\ 0 & \mathrm{X}_\tau \in \Gamma_\tau^\omega \\ -d(\mathrm{X}_\tau,\Gamma_\tau^\omega) & \mathrm{X}_\tau \in \Omega_\tau \backslash \omega_\tau \end{cases} \tag{78}$$

Here, $d(\mathrm{X}_\tau,\Gamma_\tau^\omega)$ is the distance from point X to the boundary Γ^ω, for all $\mathrm{X} \in R^n$. The R^n denotes an n-dimensional real space. Γ_τ^ω, ω_τ, and Ω_τ are the moving boundary, the corresponding domain, and the fixed reference domain at time τ, respectively. $\Phi(\mathrm{X}_\tau,\tau)$ is used to define the inside and outside regions of the interface in the domain, Ω_τ.

The approximate functions for the Heaviside and the Dirac delta functions are used:

$$H(x) = \begin{cases} \kappa & \text{if } x < -\Delta \\ \frac{3(1-\kappa)}{4}\left(\frac{x}{3} - \frac{x^3}{3\Delta^3}\right) + \frac{1+\kappa}{2} & \text{if } -\Delta < x < \Delta \\ 1 & \text{if } x \geq \Delta \end{cases} \tag{79}$$

$$\delta(x) = \begin{cases} \frac{3(1-\kappa)}{4\Delta}\left(1-\frac{x^2}{\Delta^2}\right) & \text{if } |x| \le \Delta \\ 0 & \text{if } |x| > \Delta \end{cases} \tag{80}$$

where κ is a small positive number that avoids numerical singularity, and $H(\Phi)$, $\delta(\Phi)$ is a presumed bandwidth of the Heaviside and Dirac delta functions (as shown in Fig. 3), respectively.

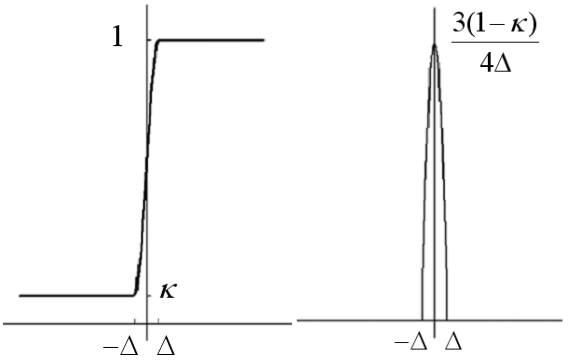

(a) Heaviside function (b) Dirac delta function

Figure 3: Approximation of functions.

6 Numerical Examples

In order to prove that the LS based optimization converges to an optimum without gray areas, a simple structural problem with a ferromagnetic material and a practical application used in industry are studied. In the former, a plate panel is excited by an external circuit current embedded in the domain. The sensitivity derived in this paper is validated using an approximate numerical approach. In this context, the optimal shapes using the level set methods are compared to the optimal pattern obtained from the conventional topology optimization (solid isotropic microstructure with penalization (SIMP) method). In the latter study, as a practical example, gray area patterns in two models using different mesh sizes are discussed through comparisons.

6.1 Verification of design sensitivity

In order to verify the accuracy of the derived sensitivity formulation, the example illustrated in Fig. 4(a) is investigated. The model has two current sources that generate a symmetric magnetic field on the domain: (+) indicates the current coming

out from the domain and (-) is the current going into the domain. The outer nodes are occupied by the homogeneous Dirichlet condition in (8). For approximate sensitivity using the finite difference method (FDM), the boundary is perturbed by 1% of the distance between a level set grid and the nearest grid. The five arbitrary points shown in Fig. 4(b) are tested for sensitivity verification. Table I shows that the adjoint variable method (AVM) is in good agreement with the FDM.

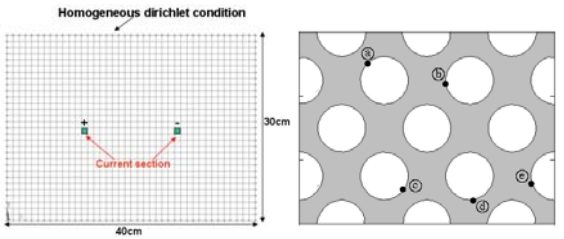

(a) (b)

Figure 4: Design domain, electric loads, and boundary conditions (a); five knots for sensitivity validation (b).

Table 1: Sensitivity Comparison between FDM and AVM

	FDM*	AVM	FDM/AVM [%]
a	5.1410E-02	5.1302E-02	100.21
b	1.9111E-01	1.9047E-01	100.34
c	5.0106E-02	4.9981E-02	100.25
d	6.5155E-02	6.5038E-02	100.18
e	5.4972E-02	5.4813E-02	100.29

* $\Delta J = \frac{J(\Phi+\Delta\Phi)-J(\Phi)}{\Delta\Phi}$, forward FDM with 1% perturbation

6.2 Example 1: Plate penal with current

In this section, the same finite element model for the sensitivity validation is used to design a plate panel. It is assumed that no magnetic vector potential leaks outward due to a homogeneous Dirichlet condition, and there is no material saturation of the material due to the fact that the linear material behavior ($\mu_r = 1000$) is used for the optimization process. This means that the design variable is considered to be independent of the magnetic flux density. Fig. 5 shows the magnetic flux contour line when the currents (positive and negative) are applied to the domain.

The ferromagnetic material is optimized to maximize the magnetic energy generated in the domain under a constraint; the allowable volume fraction is 50% of the original domain. The two methods - the conventional level set method and the advanced level set method using the RBF – are examined to compare the convergence and optimum pattern. Fig. 6 illustrates the history of the implicit boundaries evolved using the former method with initial guess holes. Fig. 7 explains the boundary history using the latter method using the RBF with the same initial holes. Fig. 8 and Fig. 9 show the optimization history of the objective function and the volume fraction for the former and the latter method, respectively. The volume fraction specified as the constraint converges at 26 iterations in the former method and at 9 iterations in the latter method. The objective function in the latter method is smoother than that of the former method during the optimization convergence. It transpires that the faster evolution occurs in the latter approach even though the resulting shapes are identical. The optimal pattern obtained from the established SIMP method [Shim, Moon, and Wang (2006)] is compared with the shape based on the advanced level set method using the RBF in Fig. 10. The SIMP method with a penalization factor of 3 yields the optimal material distribution at 18 iterations. Even though the same finite element model is used in these optimization methods, the level set method is much slower than the SIMP method because the process of merging or splitting holes requires many steps. However, it is noted that a smoother shape is obtained from the level set method.

Another initial guess that has two half holes in the upper and lower boundaries and four quarter holes in the corners are applied to the level set method. Fig. 11 illustrates the initial design and the final shapes obtained from the conventional level set method and the advanced level set method. It is found that the shapes are identical to those using the first initial guess, i.e. Fig. 6(a).

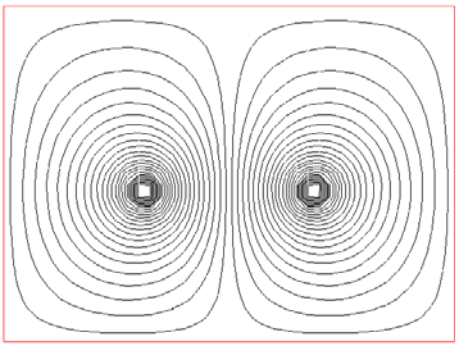

Figure 5: Magnetic flux contour plot

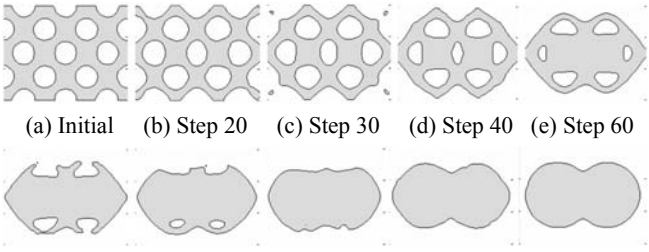

(a) Initial (b) Step 20 (c) Step 30 (d) Step 40 (e) Step 60

(f) Step 80 (g) Step 100 (h) Step 180 (i) Step 300 (j) Step 390

Figure 6: History of shape evolution using conventional level set method

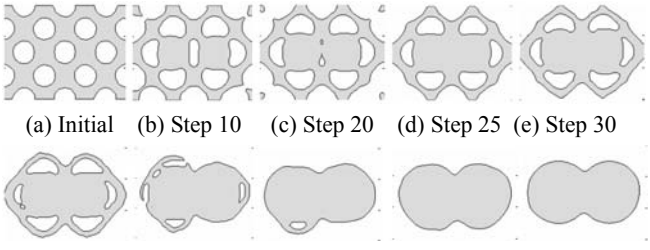

(a) Initial (b) Step 10 (c) Step 20 (d) Step 25 (e) Step 30

(f) Step 40 (g) Step 50 (h) Step 60 (i) Step 110 (j) Step 154

Figure 7: History of shape evolution using advanced level set method

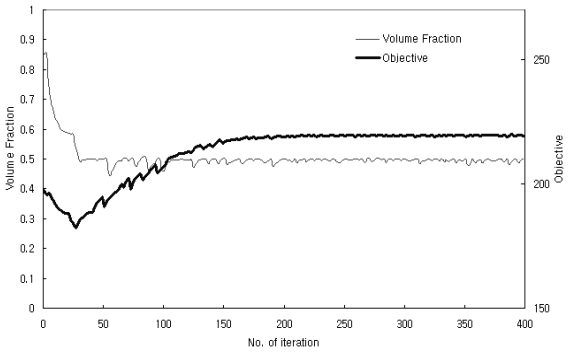

Figure 8: Optimization history of conventional level set method

6.3 Example 2: Core design used for magnetic levitation systems

The magnetic levitation (Maglev) transportation system that has evolved from linear motion development is a very promising system for the present and future. This is due to the fact that a non-contact mechanical system, through the absence of

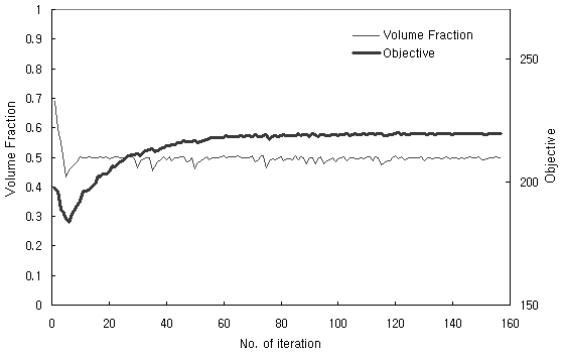

Figure 9: Optimization history of advanced level set method

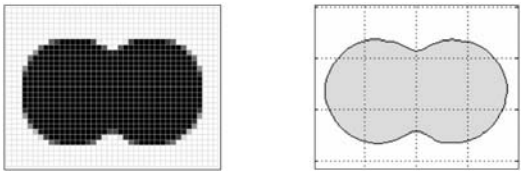

(a) Topological SIMP method (b) Advanced LSM

Figure 10: Optimal pattern of SIMP method and final shape of advanced level set method

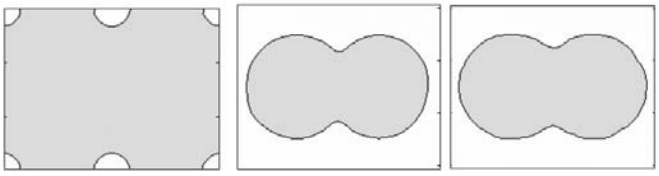

(a) Initial design (b) Conventional LSM (c) Advanced LSM

Figure 11: Initial design and final shapes with different initial design

wheels, guarantees a no-sliding operation, less noise/vibration, light weight transportation vehicles, a reduction of maintenance costs, and so on. In order to enhance the light weight structure of the vehicle body, the electromagnet must be optimized with a smaller volume constraint. The main module of the Maglev is the suspension of the vehicle body such that the levitation force is maintained equal to the original force. In this context, an example model for a magnetic levitation system is investigated using the level set methods and the topological SIMP algorithm. As shown in Fig. 12, the structure is composed of three components: a C-shaped yoke

(levitation body yoke), blade (railroad), and coil. The symbol $\otimes$ indicates a coil carrying an inflow current and $\odot$ denotes a coil carrying an outflow current. The model is symmetric so that analyzing and optimizing the half of the model is sufficient as illustrated in Fig. 12. The magnetic energy is concentrated in the air-gap because the relative permeability for ferromagnetic materials (yoke and blade) is much higher than that of air. The energy in the air-gap is the potential energy to move the structures. Thus, the model is optimized to maximize the energy generated in the air-gap. Some sections of the C-shaped yoke used for the levitation vehicle are chosen as a design domain to reduce the volume. In the optimization problem, one constraint is that the allowable volume fraction is 50% of the original domain, which is a critical criterion in maintaining the magnetic field to boost the vehicle body (C-shaped yoke). Fig. 13 presents the magnetic flux contour plot when current density (7.5E+5 $[A/m^2]$) is applied on the coil.

Fig. 14 shows the optimal patterns of the coarse model and dense model using the SIMP method in which a penalization factor of 3 results in convergence at 12 iterations and 16 iterations, respectively. The optimal pattern of the dense model is smoother, but has a broader gray band area than the coarse model. In the electromagnetic examples, the topology optimization using the SIMP method frequently results in gray areas that occupy a dominant portion of the optimal pattern. Increasing the penalization factor is able to reduce the gray region slightly, but the level of penalization is dependent on the problem type. The gray area pattern is obscure to manufacture the optimal design, so it requires post processing to convert the solid-void pattern with distinct boundaries, i.e. all densities in an optimal pattern are either 0 or 1. There are two possible approaches for the post processing. The first is that the designer is able to create an optimal model intuitively from final pattern with the gray areas. The second approach applies a threshold to separate either solid or void material. In order to make a solid-void design in this paper, a density of 0.5 is applied as the threshold. Once the material density (design variable in the SIMP method) of the design element is greater than 0.5, it is selected as an optimal domain, i.e. a solid domain. Fig. 15 shows the final shape after the post processing.

Fig. 17 shows the final resulting shapes of the conventional level set method and the advanced level set method using the initial guesses illustrated in Fig. 16. The final shape of the former method converges in the local optimal shape, which is far from the global optimum obtained using the SIMP method. However, the final shape of the latter method is closer to that of the SIMP method by making the gray area band free.

The design built after the post processing is re-analyzed to be compared with the results of the level set method. Table II explains that the re-analysis results of the topological SIMP method are close to the advanced level set method only. Thus, the

advanced level set method using the RBF is applicable to practical electromagnetic problems.

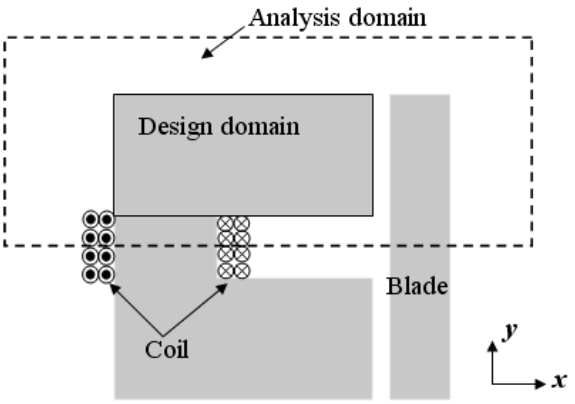

Figure 12: Magnetic levitation system and design domain

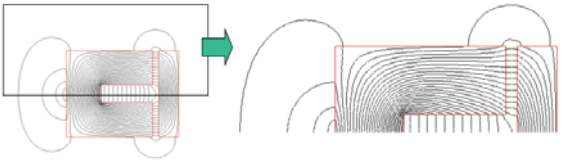

Figure 13: Magnetic flux contour plot

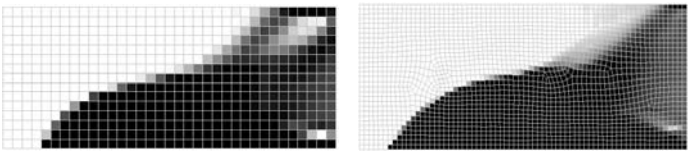

(a) Coarse model (b) Dense model

Figure 14: Optimal patterns of SIMP method

7 Conclusions

A topological shape optimization method has been developed for electromagnetic problems in a steady state using the level set method. Since implicit moving bound-

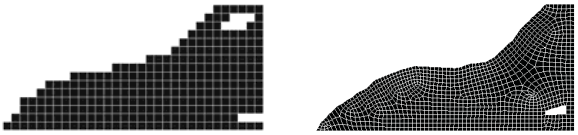

(a) Coarse model (b) Dense model

Figure 15: Final shape after post processing

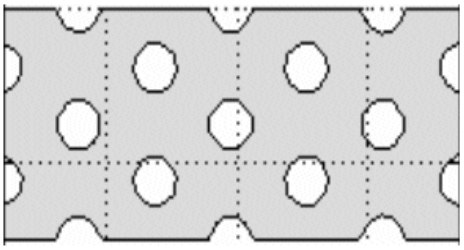

Figure 16: Initial design for level set method

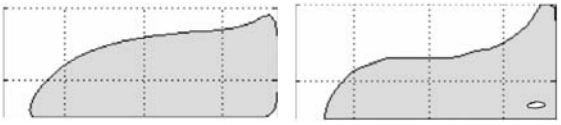

(a) Conventional LSM (b) Advanced LSM

Figure 17: Final shape using level set methods

Table 2: Comparison of objective values

Type	Objective value [J/m^3]
SIMP method – coarse model	Optimal pattern: 149.53 Final shape after post processing: 149.42
SIMP method – dense model	Optimal pattern: 149.74 Final shape after post processing: 149.73
Conventional level set method	Final shape: 143.64
Advanced level set method	Final shape: 149.72

aries are used to show the design contours, it is not only easy to represent the shape variation, but also unnecessary to carry out re-mesh generation after significant shape changes during the optimization process. The boundary velocity to integrate the Hamilton-Jacobi equation is obtained from the Kuhn-Tucker optimality condi-

tion for the Lagrangian function. The design sensitivity equation employing the adjoint variable method is emphasized by verifying its accuracy compared with the finite difference method in a simple example. It reduces the numerous gradient evaluations providing the optimizer with the best direction in the next iteration.

Based on numerical examples, it is shown that the advanced level set method using the RBF yields a similar optimal shape to the established SIMP approach and converges to the optimum faster and smoother than the conventional level set method. The removal of the gray areas is achieved in the level set based optimization such that the additional work (i.e. post processing) is not required. Moreover, the level set method is able to result in smooth boundaries. However, it is noted that the computation cost is considerably expensive in comparison with the SIMP method.

References

Allaire, G.; Jouve, F.; Toader, A. (2002): A level set method for shape optimization. *C.R. Acad. Sci. Paris, Ser. I*, Vol. 334, pp. 1125-1130.

Allaire, G.; Jouve, F.; Toader, A. (2004): Structural optimization using sensitivity analysis and a level-set method. *Journal of Computational Physics*, Vol. 194, pp. 363-393.

Arora, J. S. (1989): Introduction to optimum design, McGraw-Hill, New York.

Bendsoe, M. P.; Kikuchi, N. (1988): Generating optimal topologies in structural design using a homogenization method. *Computer Method in Applied Mechanics and Engineering*, Vol. 71, pp. 197-224.

Bendsoe, M. P. (1995): Optimization of structural topology, shape, and material, Springer-Verlag, Berlin Heidelberg.

Bendsoe, M. P.; Sigmund, O. (2003): Topology Optimization – Theory, Methods and Application. Springer.

Burger, M.; Hackl, B.; Ring, W. (2004): Incorporating topological derivatives into level set methods. *Journal of Computational Physics*, Vol. 194, pp. 344-362.

Cheng, A. D.; Golberg, M. A.; Kansa, E. J.; Zammito, G. (2003): Exponential convergence and H-c multiquadric collocation method for partial differential equations. *Numerical Methods for Partial Equation*, Vol. 19, Issue. 5, pp. 571-594.

Cisilino, Adri ' a n P. (2006): Topology optimization of 2D potential problems using boundary elements. *CMES: Computer Modeling in Engineering & Sciences*, 15(2), pp. 99-106.

Franke, R. (1982): Scattered data interpolation: Test of some methods. *Mathematics of Computation*, Vol. 38, pp. 181-200.

Frei, W.; Tortorelli, D.; Johnson, H. (2007): A geometry projection method for

optimizing photonic nanostructures. *Optics Letters*, Vol. 32, No. 1, pp. 77-79.

Haug, J.; Choi, K.; Komkov, V. (1986): Design Sensitivity Analysis of Structural Systems, Academic Press, Inc..

Jiang, G. S.; Peng, D. (2000): Weighted ENO schemes for Hamilton-Jacobi equation. *SIAM Journal on Scientific Computing*, Vol. 21, pp. 2126-2143.

Juan, Z.; Shuyao, L.; Yuanbo, X; Guangyao, L. (2008): A topology optimization design for the continuum structure based on the meshless numerical technique. *CMES: Computer Modeling in Engineering & Sciences*, 34(2), pp. 137-154.

Li, S.; Atluri, S. N. (2008a): Topology-optimization of structures based on the MLPG mixed collocation method. *CMES: Computer Modeling in Engineering & Sciences*, 26(1), pp. 61-74.

Li, S.; Atluri, S. N. (2008b): The MLPG mixed collocation method for material orientation and topology optimization of anisotropic solids and structures. *CMES: Computer Modeling in Engineering & Sciences*, 30(1), pp. 37-56.

Luo, Z.; Wang, M. Y.; Wang, S. Y.; Wei, P. (2008): A level set-based parameterization method for structural shape and topology optimization, *International Journal for Numerical Methods in Engineering*, 76(1), pp. 1-26.

Norato, J.; Haber, R.; Tortorelli, D.; Bendsoe, M. P. (2004): A geometry projection method for shape optimization. *International Journal for Numerical Methods in Engineering*, Vol. 60 (14), pp. 2289-2312.

Osher, S.; Sethian, J. A. (1988); Front propagating with curvature dependent speed: algorithms based on Hamiton-Jacobi formulations. *Journal of Computational Physics*, Vol. 78, pp. 12-49.

Salon, S. J. (1998): Finite Element Analysis of Electrical Machines, Kluwer Academic Publishers, Second Printing, Massachusetts, USA.

Sethian, J. A.; Wiegmann, A. (2000): Structural boundary design via level set and immersed interface methods. *Journal of Computational Physics*, Vol. 163, pp. 489-528.

Shim, H.; Moon, H.; Wang, S. (2006): 3D topology optimization of magneto-thermal systems. *COMPEL*, Vol. 25, No. 3, pp. 572-580.

Shim, H.; Moon, H.; Wang, S.; Hameyer, K. (2008): Topology optimization for compliance reduction of magneto-mechanical systems. *IEEE Transactions on Magnetics*, Vol. 44, No. 3, pp. 346-351.

Shim, H.; Wang, S.; Hameyer, K. (2007): Topology optimization of magnetothermal systems considering eddy current as Joule heat. *IEEE Trans. Magn.*, Vol. 43, No. 4, pp. 1617-1620.

Sigmund, O. (2001): Design of multiphysics actuators using topology optimization – part II: two material structures. *Comput. Methods Appl. Mech. Engrg.*, Vol. 190, pp.6605-6627.

Sigmund, O.; Petersson, J. (1998); Numerical instabilities in topology optimization: A survey on procedures dealing with checkerboards, mesh-dependencies, and local minima. *Structural Optimization*, Vol. 16, pp. 68-75.

Sokolowski, J.; Zolesio, J. P. (1992): Introduction to shape optimization: shape sensitivity analysis. In Springer Series in Computational Mathematics, Vol. 10, Springer, Berlin, Germany.

Wang, M. Y.; Wang, X.; Guo, D. (2003): A level set method for structural topology optimization. *Computer Methods in Applied Mechanics and Engineering*, Vol. 192, pp. 227-246.

Wang, S. Y.; Wang, M. Y. (2006a): Radial basis functions and level set method for structural topology optimization. *International Journal for Numerical Methods in Engineering*, Vol. 65. Issue. 12, pp. 2060-2090.

Wang, S. Y.; Wang, M. Y. (2006b): Structural shape and topology optimization using an implicit free boundary parameterization method. *CMES: Computer Modeling in Engineering & Sciences*, Vol. 13, No. 2, pp. 119-147.

Wang, S. Y.; Lim, K. M.; Khoo, B. C.; Wang, M. Y. (2007a): A geometric deformation constrained level set method for structural shape and topology optimization. *CMES: Computer Modeling in Engineering & Science*, 18(3), pp. 155-181.

Wang, S. Y.; Lim, K. M.; Khoo, B. C.; Wang, M. Y. (2007b): An unconditionally time-stable level set method and its application to shape and topology optimization. *CMES: Computer Modeling in Engineering & Science*, 21(1), pp. 1-40.

Wang, S. Y.; Lim, K. M.; Khoo, B. C.; Wang, M. Y. (2007c): An extended level set method for shape and topology optimization. *Journal of Computational Physics*, Vol. 221, pp. 395-421.

Wang, S. Y.; Lim, K. M.; Khoo, B. C.; Wang, M. Y. (2007d): On hole nucleation in topology optimization using the level set methods. *CMES: Computer Modeling in Engineering & Sciences*, Vol. 21, pp. 219-237.

Wang, S. Y.; Lim, K. M.; Khoo, B. C.; Wang, M. Y. (2008): A hybrid sensitivity filtering method for topology optimization. *CMES: Computer Modeling in Engineering & Science*, 24(1), pp. 21-55.

Xia, Q.; Wang, M. Y. (2008): Topology optimization of thermoelastic structures using level set method. *Computational Mechanics*, 42(6), pp. 837-857.

Yoon, G.; Kim. Y. (2005): The element connectivity parameterization formulation for the topology design optimization of multiphysics systems. *Int. J. Numer. Meth.*

Engrg., Vol. 64, pp. 1649-1677.

Zhou, S. W.; Wang, M. Y. (2006): 3D multi-material structural topology optimization with the generalized Cahn-Hilliard equations, *CMES: Computer Modeling in Engineering & Sciences*, 16(2), 83-102.